Geophysical Research Letters

RESEARCH LETTER
10.1029/2021GL092968

3D Modeling of Long-Term Slow Slip Events Along the Flat-Slab Segment in the Guerrero Seismic Gap, Mexico

Andrea Perez-Silva[1,2], Duo Li[1], Alice-Agnes Gabriel[1,3], and Yoshihiro Kaneko[4]

[1]Department of Earth and Environmental Sciences, Ludwig-Maximilians-Universität München, München, Germany, [2]Now at Victoria University of Wellington, School of Geography, Environment and Earth Sciences, Wellington, New Zealand, [3]Scripps Institution of Oceanography, University of California San Diego, San Diego, CA, USA, [4]Department of Geophysics, Graduate School of Science, Kyoto University, Kyoto, Japan

Key Points:

- We model sequences of long-term slow slip events in the Guerrero Seismic Gap using a geometrically flexible three-dimensional (3D) boundary integral method
- Our model reproduces the source characteristics and surface deformation of the four long-term slow slip events (SSEs) inferred from geodetic observations
- The flat segment of the Cocos plate likely aids the large magnitudes and long recurrence interval of the slow slip events in Guerrero

Supporting Information:

Supporting Information may be found in the online version of this article.

Correspondence to:

D. Li,
dli@geophysik.uni-muenchen.de

Citation:

Perez-Silva, A., Li, D., Gabriel, A.-A., & Kaneko, Y. (2021). 3D modeling of long-term slow slip events along the flat-slab segment in the Guerrero Seismic Gap, Mexico. *Geophysical Research Letters*, *48*, e2021GL092968. https://doi.org/10.1029/2021GL092968

Received 25 FEB 2021
Accepted 8 JUN 2021

Abstract During the last two decades, quasi-periodic long-term slow slip events (SSEs) of magnitude up to M_w7.5 have been observed about every 4 years in the Guerrero Seismic Gap, Mexico. We present numerical simulations of the long-term SSE cycles along the 3D slab geometry of central Mexico. Our model accounts for the hydrated oceanic crust in the framework of rate-and-state friction and captures the major source characteristics of the long-term SSEs occurring between 2001 and 2014, as inferred from geodetic observations. Synthetic surface deformation calculated from simulated fault slip is in good agreement with the cumulative GPS displacements. Our results suggest that the flat-slab segment of the Cocos plate aids the large magnitudes and long recurrence interval of the long-term SSEs. We conclude that 3D slab geometry is an important factor in improving our understanding of the physics of slow slip events.

Plain Language Summary Slow slip events (so-called "silent earthquakes") have been detected worldwide in circum-Pacific subduction zones, such as Cascadia and southwest Japan. Long-term slow slip events occur about every 4 years in the Guerrero Seismic Gap (Mexico) where tectonic plate movement is largely accommodated by aseismic slip and no large earthquakes have been observed since 1911. We build a numerical model incorporating a realistic 3D geometry of the subducting slab and lab-derived friction laws to investigate the physics of these slow slip events. The simulated events have slip patterns, magnitudes, and recurrence intervals comparable with the observed ones. Our study demonstrates that plate geometry is an important factor to account for when studying the initiation, propagation and arrest of slow slip.

1. Introduction

Slow slip events (SSEs) are recurring and transient periods of aseismic slip on plate interfaces. SSEs occur predominantly at the edges of the seismogenic zone where the frictional regime transitions from stick–slip to stable-sliding behavior (Dragert et al., 2001; Peng & Gomberg, 2010; Radiguet et al., 2012; Schwartz & Rokosky, 2007; Wallace & Beavan, 2010). The discovery of SSEs has transformed our perception of how the long-term geological loading is released along plate boundaries, as these events can account for a significant fraction of the accumulated strain (Peng & Gomberg, 2010; Radiguet et al., 2012; Schwartz & Rokosky, 2007; Wallace & Beavan, 2010). Observations, numerical modeling, and laboratory experiments suggest that several factors, such as pore fluid pressure, thermal structure, rock composition, slab geometry, and rheological complexity, may influence the dynamics of SSEs (Audet et al., 2009; Hyndman, 2013; Li & Liu, 2016; Liu & Rice, 2005; McLaskey & Yamashita, 2017; Saffer & Wallace, 2015; Scholz, 1998; Wech & Creager, 2011; Wei et al., 2013, 2018).

In central Mexico, long-term SSEs (Schwartz & Rokosky, 2007), which are commonly defined as having long duration (on the order of years), large magnitude ($M_w > 6.5$) and long recurrence intervals (2–10 years), have been detected over the last two decades (Kostoglodov et al., 2003; Radiguet et al., 2012; Vergnolle et al., 2010). These SSEs (Figure 1) occur in the northwestern part of the Guerrero Seismic Gap (GSG), which is a 100-km segment that has not experienced any large earthquakes ($M_w > 7.0$) since 1911 (Kostoglodov et al., 2003; Rudolf-Navarro et al., 2010). Continuous GPS measurements show that they occur every ~4 years and last from several months up to one year. These aseismic events release elastic energy

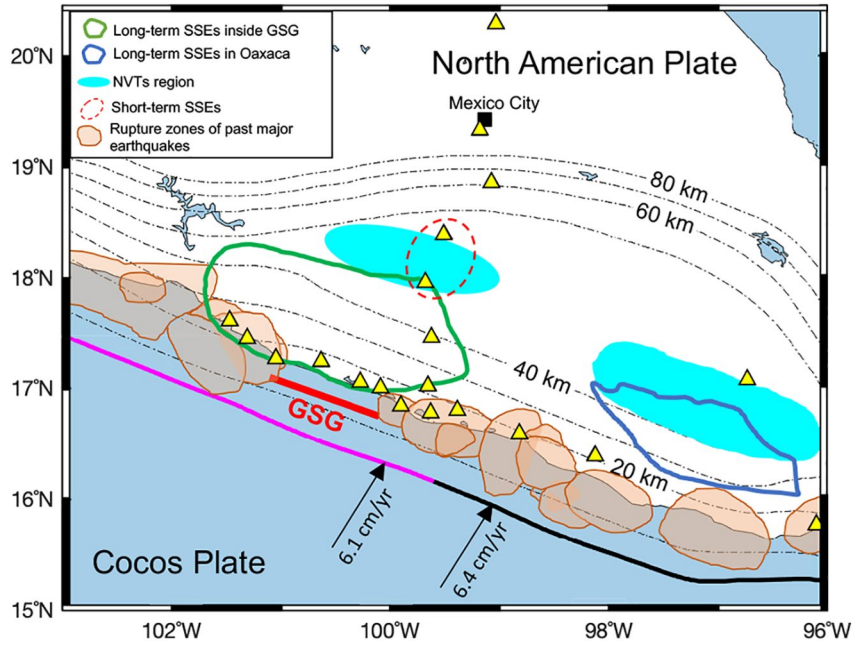

Figure 1. Map of the Mexico subduction zone defined by the convergence of the Cocos and North American plates. The red bar highlights the northwestern portion of the Guerrero Seismic Gap extending 100 km along the strike. Orange patches indicate the rupture area of major thrust earthquakes (adapted from Figure 1 in Radiguet et al. (2012). Black arrows show direction and rate (in cm/yr) of plate convergence (DeMets et al., 2010). The green contour represents the 20 cm cumulative slip contour of SSEs in 2001/2002, 2006, and 2010 from Radiguet et al. (2012). The blue contour denotes the location of SSEs in the Oaxaca segment from Fasola et al. (2016). Cyan patches show the regions of NVTs (after Figure 1 Husker et al. (2019)). The dashed red line shows the 4 mm slip contour of a short-term SSE (Villafuerte & Cruz-Atienza, 2017). Black dashed lines indicate the 10-km spacing depth contours of the Cocos plate from Pérez-Campos et al. (2008), with tags at every 20 km. Yellow triangles denote regional permanent GPS stations. The thick black line indicates the location of the trench; its magenta part highlights the along-strike extension of the model geometry used in this study and detailed in Figure 2. Mexico City is shown as a black square.

equivalent to up to ~M_w7.5 earthquakes (Kostoglodov et al., 2003; Lowry et al., 2001; Radiguet et al., 2012), ranking among the largest SSEs worldwide. Smaller (M_w 6.6–6.9) and more frequent (1–2 years) SSEs occur in Oaxaca state (Graham et al., 2016), ~300 km southeastward of GSG (Figure 1). Short-term SSEs of small magnitude and short recurrence interval (M_w ~ 6.4, 3 months) and non-volcanic tremors (NVTs, in the frequency range of 1–10 Hz) have been identified in the vicinity of the downdip edge of the long-term SSEs in Guerrero (Frank et al., 2015; Husker et al., 2012, 2019; Maury et al., 2018; Villafuerte & Cruz-Atienza, 2017). All of these observations highlight the diversity of slow slip behavior in central Mexico.

Receiver functions and seismic velocity tomography along the broadband Meso-American Subduction Experiment (MASE) array (MASE, 2007) reveal a horizontal segment of the downgoing Cocos plate beneath the Guerrero region (Husker & Davis, 2009; Kim et al., 2010; Pérez-Campos et al., 2008). This flat-slab segment may be due to ongoing continental crust hydration and weakening, a process that started 15 Ma ago (Manea & Manea, 2011). High pore fluid pressure has been inferred atop the horizontal segment (Jödicke et al., 2006; Kim et al., 2010; Song et al., 2009), which may result in a favorable environment for SSEs and NVTs (Song et al., 2009; Manea & Manea, 2011).

The effect of slab geometry has been studied in previous non-planar rate-and-state friction modeling of SSEs in the Nankai, Cascadia, eastern Alaska and Hikurangi subduction zones (Li & Liu, 2016, 2017; Li et al., 2018; Matsuzawa et al., 2013; Shibazaki et al., 2012, 2019). Here we investigate the importance of 3D variations in slab geometry for the dynamics of SSEs in Guerrero. We perform numerical simulations of long-term SSEs using realistic 3D slab geometry of the Cocos plate in central Mexico. We compare modeled long-term SSE source characteristics and surface deformation with geodetic inversion results from two-decade-long continuous GPS records. Our model has important implications for our understanding of the physics of long-term SSEs in relation to slab geometry and fault strength.

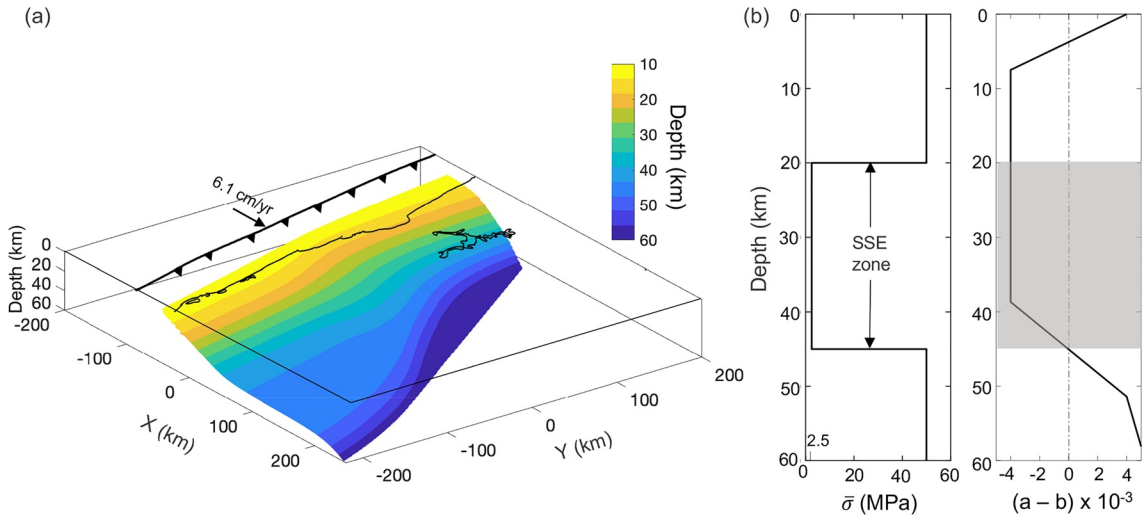

Figure 2. (a) Diagram of the 3D non-planar Cocos plate based on Pérez-Campos et al. (2008). The fault extents 430 km along the strike (see magenta line in Figure 1) and from 10 to 60 km in depth. The black arrow indicates relative plate motion (in cm/yr) taken from the PVEL model (DeMets et al., 2010). The black jagged line indicates the trench. (b) Depth profiles of effective normal stress ($\bar{\sigma}$) and friction parameter (a–b). The *SSE zone* refers to the depth range where $\bar{\sigma}$ = 2.5 MPa. The gray shaded area represents the velocity-weakening region ($a - b < 0$) under low effective normal stress.

2. Methods and Model Setup

To model SSE cycles, we use the code developed by Li and Liu (2016). There are three main ingredients to this approach: (a) a quasi-dynamic formulation of traction and slip as defined by Rice (1993), (b) the fault constitutive response is given by a laboratory-derived rate-and-state friction law, and (c) it enables to incorporate non-planar, 3D fault geometry. We describe each ingredient in detail in the Supplementary Text S1.

We incorporate 3D plate geometry of the Cocos plate inferred from a dense broadband seismic array experiment (Pérez-Campos et al., 2008). The model domain extends 430 km along the Cocos-North America plate boundary and covers a depth range from 10 to 60 km (Figure 2a). The slab is assumed locked from the trench to 15 km depth by imposing zero slip boundary conditions. While near-trench observations such as seafloor geodesy data is lacking, we base this assumption on the shallow locations of historical major thrust earthquakes (Figure 1) and the updip limit of inverted SSE distributions (Radiguet et al., 2016). We define a uniform plate convergence velocity that is directed N63°E at a rate of V_{pl} = 6.1 cm/yr (DeMets et al., 2010). The slab geometry is discretized into triangular elements with edge lengths no longer than 1,500 m using the commercial software Cubit/Trelis (https://www.coreform.com/).

The friction parameter ($a - b$) is adapted from frictional experiments in wet gabbro gouges (He et al., 2007) and mapped onto the 3D slab interface (Figure 2b) based on the thermal structure beneath Central Mexico (Manea & Manea, 2011). Velocity-strengthening (VS) conditions ($a - b > 0$) are also imposed at the edges of the model domain to stabilize slip at the plate convergence rate (Figure S1). The assumption of a VS band at the eastern end of the model is based on geodetic coupling estimates that indicate a low long-term coupling in the region eastward from the 2014 SSE (Radiguet et al., 2016). We demonstrate that the slip rate evolution does not change significantly in an alternative model setup without velocity-strengthening bands at the edges of the model domain (Text S3, Figure S8).

Following previous studies (e.g., Liu & Rice, 2007; Li & Liu, 2016; Shibazaki et al., 2019), we account for the inferred high pore fluid pressure condition atop the Cocos plate where SSEs occur (Jödicke et al., 2006; Kim et al., 2010; Song et al., 2009) by assuming low effective normal stress $\bar{\sigma}$ within the SSE source region. $\bar{\sigma}$ is set to be 2.5 MPa from 20 to 45 km depth and it is 50 MPa elsewhere. We refer to the depth range of low $\bar{\sigma}$ as the "SSE zone" (Figure 2b). The model parameter W is defined as the downdip width of the SSE zone under velocity-weakening conditions (Figure 2b).

The ratio W/h^*, where h^* is the critical nucleation size given by the definition of Rubin and Ampuero (2005) (Text S1), has been shown to be a key parameter that controls the periodic behavior of the fault and the

emergence of SSEs (Barbot, 2019; Liu & Rice, 2007). Previous studies have also shown that $W/h^* \sim 1$ reproduces slow slip characteristics in Cascadia (Liu & Rice, 2007; Li & Liu, 2016). Here we vary W and h^* independently and report the source properties (recurrence, magnitude and slip velocity) for each parameter configuration (Figures S3 and S4). Specifically, we explore various W by assuming different updip limiting depths of the SSE zone (Text S2). The simulation assuming $W/h^* = 1.18$ ($d_c = 10.1$ mm) is selected as the preferred model since it best reproduces the characteristics and geodetic signature of long-term SSEs in Guerrero. In the following we describe the results of this simulation. Other parametrizations and the respective sensitivities are discussed in Supplementary Text S2.

Of the preferred SSE cycle model we select four events as representative of the observed long-term SSEs in Guerrero and calculate their synthetic surface deformation. The required Green's functions are calculated assuming a homogeneous elastic half-space and implemented for triangular dislocation elements using the MATLAB code developed by Meade (2007).

3. Results

3.1. Spatio-Temporal Evolution of Slip Rate

The model produces spontaneous slow slip events under constant plate loading until 145 years, at which time we terminate the simulation at the appearance of a seismic event ($V > 5$ mm/s). This earthquake's peak velocity occurs at 35 km depth (i.e., within the SSE zone) and is omitted in the following analysis since there is no observational evidence for such an event in the Guerrero Seismic Gap, yet. However, from previous planar fault SSE models (Liu & Rice, 2007) we expect that the major source characteristics of later SSEs would not be affected by the emergence of earthquakes in case these are separated by several years.

The slip rate of the modeled SSEs varies by several orders of magnitude on the fault (Figure 3a). Rupture migrating fronts where $V > 3V_{pl}$ (red contours in Figure 3a) indicate the occurrence of slow slip events. In the time interval between these events the fault is locked with slip velocities ranging from $0.03V_{pl}$ to $0.3V_{pl}$ (dark blue areas in Figure 3a).

In this model, we identify three types of SSEs with different along-strike extent. Type I events rupture most of the slab along-strike, extending approximately 300 km (green arrows in Figure 3a). The evolution of these events starts with a slow nucleation phase that takes place close to VS-VW transition at two distant locations ($y = 150$ km and $y = -150$ km), from which two slip fronts migrate toward each other (convergent yellow arrows in Figure 3a). These slip fronts merge into a velocity peak ($V_{max} > 10^3\ V_{pl}$) that occurs at ~35 km depth; afterward they propagate bilaterally along-strike (divergent yellow arrows in Figure 3a) and along-dip (both updip and downdip). The downdip-migrating slip front propagates across the flat-slab segment. During this propagation phase, the peak velocities of the slip fronts progressively decrease. The migration fronts of these events are asymmetric, in that the slip front migrates slightly slower and over a longer distance eastwards than westwards.

Type II events (black arrows in Figure 3a) show a similar evolution pattern to Type I SSEs, except for a shorter along-strike extent (150–200 km) and a more symmetric migration path. Type III events have the shortest along-strike extent (<100 km) (red arrows in Figure 3a) and the lowest peak slip rates, $V_{max} < 10^2\ V_{pl}$. Type II and Type III events may occur close to each other in space and time (e.g., the SSE during year ~20 in Figure 3a) and in this case two distinct velocity peaks arise (Movie S3).

The peak slip rates during SSEs appear at different along-strike locations; peak velocities arise mostly in the eastern part of the fault ($y < 0$ km) for Type I and II SSEs and in the western part ($y > 0$ km) for Type III SSEs. This difference is important as most of the final slip accumulates during the period of peak slip velocities. Thus, the final slip of Type I and II SSEs concentrates in the eastern part of the fault, while for Type III it concentrates on the western part of the fault.

The magnitude and recurrence interval of peak slip rates also vary along the strike. The history of slip rates at two points (P1 and P2, colored circles in Figures 3a and 3d) is shown in Figure 3c, respectively. Peak slip velocities at P2 are 1–2 orders of magnitude lower than those at P1. The time interval between two sequential peaks is shorter at P2 (~2–3 years) than that at P1 (~4 years). The along-strike change in the slip rate evolution intensifies in the next 50 simulation years (Figure S5a), where Type III SSEs persistently emerge

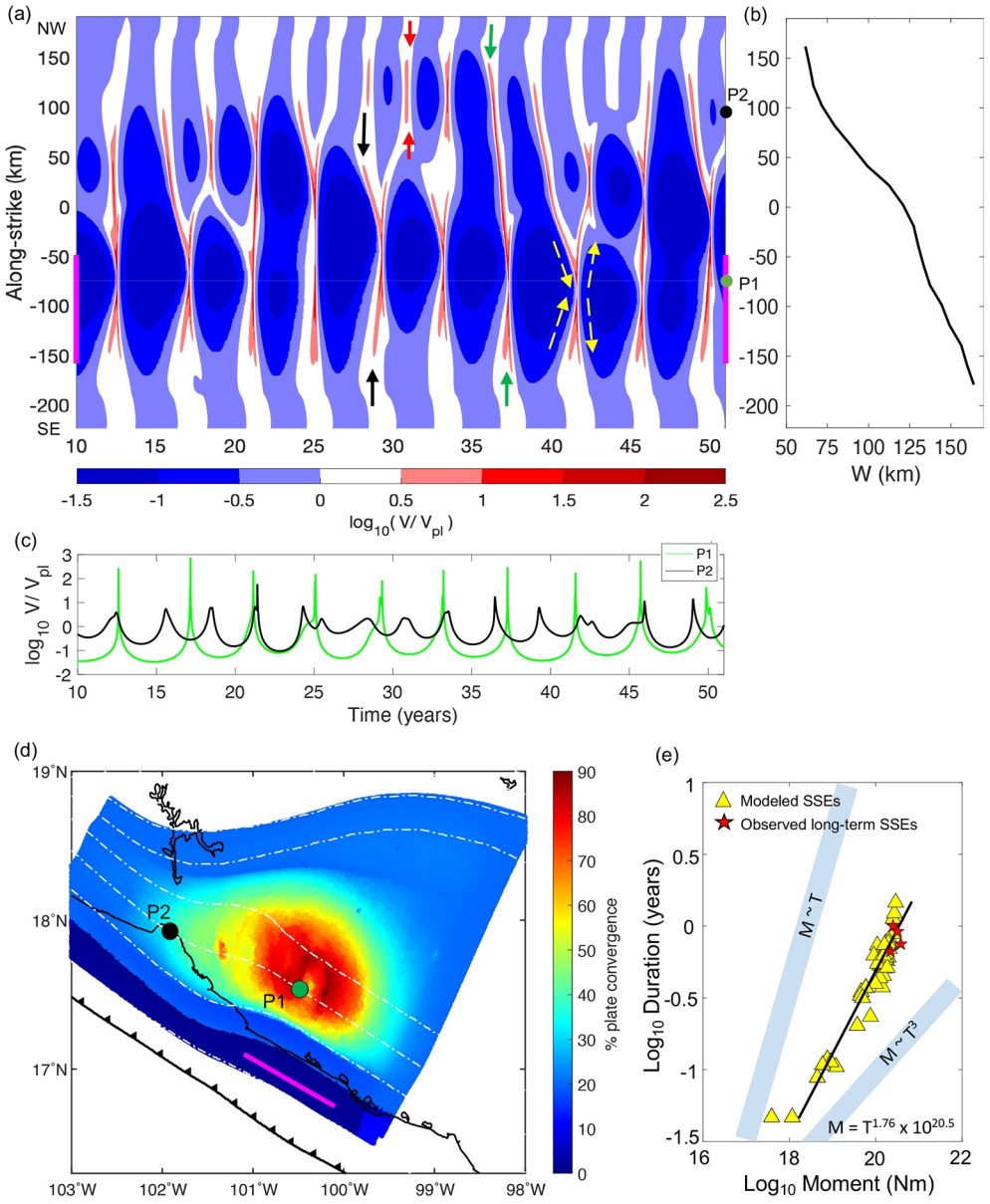

Figure 3. (a) Spatio-temporal evolution of slip rate at 30 km depth in $\log_{10}(V/V_{pl})$ scale. Thick magenta lines indicate the northwestern GSG. Green, black and red arrows point to the three types of SSEs described in the text. Dashed yellow arrows indicate the migration of slow slip fronts. (b) W (downdip distance on the fault surface) along-strike for the SSE zone between 20 and 45 km depth. (c) Slip rate at points P1 and P2 over the same period shown in (a) (location of P1 and P2 shown in (a) and (d)). (d) Slip released by long-term SSEs over 20 years as a percentage of total plate convergence. The dashed white line outlines the depth contours from 20 to 60 km depth. The magenta line highlights the location of the GSG. Green and black colored circles indicate locations of points P1 and P2, respectively. (e) Moment-duration scaling relation of 47 modeled SSEs over 145 simulation years (yellow triangles). Red stars indicate the data from four long-term SSEs in Guerrero (2001/2002, 2006, 2009/2010, 2014) taken from Radiguet et al. (2012, 2016). Best fit scaling of modeled SSEs shown in black ($M \sim T^{1.76}$). $M \sim T$ and $M \sim T^3$ scaling are shown as reference.

in the western part of the fault (between 50 to 150 km along-strike); whereas Type I and II events concentrate further to the east.

3.2. Comparison With Geodetic Observations

We compare simulated SSEs in the preferred model with those estimated from geodetic inversion in terms of duration, magnitude and recurrence interval. We select the modeled SSEs in the time period between 10 to 50 years that occur within the GSG and calculate their source properties assuming a slip rate threshold of $10V_{pl}$ (i.e., 61 cm/yr or $10^{-7.7}$ m/s). The SSE duration is defined as the time period over which this slip velocity threshold is exceeded. We then calculate the total cumulative slip and moment magnitude within the estimated duration. The recurrence interval is given by the time between peak slip rates of successive SSEs. We assume a minimum slip of 1 cm to calculate the SSE magnitude, consistent with the threshold used in geodetic inversion (Radiguet et al., 2012).

Our modeled SSEs capture the major characteristics of the four long-term SSEs that occurred in 2001/2002, 2006, 2009/2010 and 2014, as inferred from geodetic inversion. They have an average duration, magnitude and recurrence interval of 8.7 ± 3 months, M_w7.44 ± 0.08, and 4.2 ± 0.2 years, respectively; all within the range of observations (Graham et al., 2016; Radiguet et al., 2012, 2016), as shown in Table S1. Figure S2 shows daily time series at GPS station CAYA, located along the Guerrero coast, and the cumulative slip at a fault node projected vertically from the station. The modeled recurrence interval agrees well with that indicated by the permanent geodetic records.

To further validate the modeled SSEs, we show in Figure 4 the slip distribution of four modeled SSEs that best capture the characteristics of the four long-term SSEs in Guerrero. Movies S1–S4 show the spatial and temporal evolution of the slip rate on the fault during these events. The synthetic surface deformation of modeled SSEs (red arrows in Figure 4) is calculated as described in Section 2. To quantify the comparison between observed and modeled surface displacement, we define a misfit function as

$$\chi^2 = \frac{1}{N}\sum_{j=0}^{N}\left|\overrightarrow{S_j}^{obs} - \overrightarrow{S_j}^{mod}\right|^2, \tag{1}$$

where $\vec{S}^{mod}$ and $\vec{S}^{obs}$ are the modeled and observed GPS displacement vectors at the jth station and N is the number of stations that detect the SSEs within our model domain. We report the respective misfits in Figure 4. The synthetic vectors match magnitude and direction of observations reasonably well, although the direction of the horizontal components along the coast shows a slight anti-clockwise rotational offset. The latter may indicate a strike-slip component, which contributes to the observed displacements. This component is not captured by our model, as we assume pure trench-normal slip.

The modeled SSEs exhibit along-strike migration rates of 0.5 ± 0.3 km/day, which is comparable to the slow migration speeds (0.8 km/day) reported for the 2006 SSE (Radiguet et al., 2011), but lower than the 6–9 km/day estimated during the 2002 SSE (Kostoglodov et al., 2003). Low migration speeds, close to our model results, have also been reported for both observed and modeled long-term SSEs in Upper Cook Inlet in Alaska (Fu et al., 2015; Li et al., 2018), and in southwest Japan (Liu et al., 2010).

3.3. Long-Term Slip Budget

To estimate the long-term slip budget within the GSG from our model, we sum up the total cumulative slip released by long-term SSEs over 20 years and divide it by the total amount of slip accumulated due to plate convergence over the same period. The total slip released (Figure 3d) is calculated as follows:

$$\xi = \left(V_{pl}T\right)^{-1}\sum_{i=1}^{N}\delta_i, \tag{2}$$

where $N = 5$ and δ_i are the number of SSE episodes and the cumulative slip of each episode, respectively, and $T = 20$ years. The slip deficit equals to $1 - \xi$.

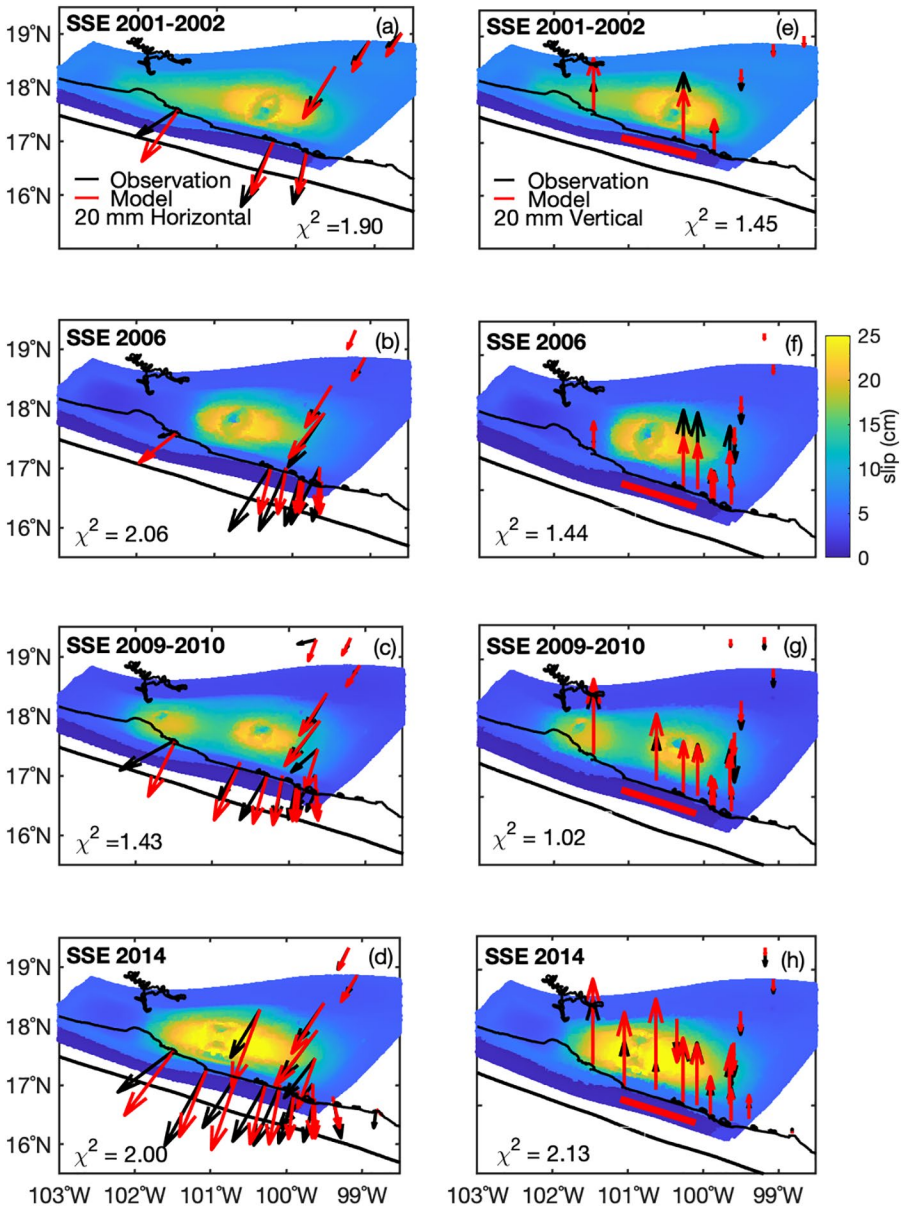

Figure 4. Modeled slip distribution of four simulated SSEs and comparison between synthetic (red) and observed (black) GPS displacement vectors of the four SSE episodes of 2001/2002 (a and e), 2006 (b and f), 2009/2010 (c and g) and 2014 (d and h). (a)–(d) Horizontal surface displacements of the four episodes, respectively. Black arrows are GPS displacements inferred from observation (Gualandi et al., 2017; Radiguet et al., 2012). Red arrows are synthetic GPS displacements. (e)–(h) Vertical surface displacements. The thick red line indicates the GSG. The thick black line denotes the Middle American Trench. Depth contours are the same as in Figure 3d. Each plot reports χ^2, the misfit of synthetic and observational data, as defined in Equation 1.

We find that within the GSG, the fault releases >80% of the plate convergence loading via slow slip. This result is comparable to the geodetic estimate in Radiguet et al. (2012), which indicate that SSEs release 75% of the accumulated strain within the GSG over three SSE cycles. The slip budget varies minimally if we consider a time interval of 40 years to calculate the slip budget (Figure S6).

3.4. Moment-Duration Scaling Relation

We calculate the moment-duration scaling relation of the modeled SSEs (triangles in Figure 3e) assuming a velocity threshold of $10V_{pl}$ (i.e., 61 cm/yr) and a threshold slip of 1 cm to calculate the moment. The best-fit scaling of the modeled SSEs follows $M \sim T^{1.76}$. The moment and duration of the four long-term SSE episodes reported by Radiguet et al. (2012, 2016) fall within the upper bound of our model (red stars in Figure 3e). The wider range in magnitude and duration of modeled SSEs may result from the different spatio-temporal behaviors of all three types of SSEs as described in Section 3.1. This scaling relation changes only slightly when including more events with different h^* values ($M \sim T^{1.56}$ in Figure S7a). Assuming a noise-free slip threshold of 3 V_{pl}, we find a slightly reduced exponent of 1.34 (Figure S7b).

4. Discussion

4.1. Geometric Effects on the Source Properties of SSEs

The emergence of long-term SSEs of large magnitudes, $M_w \geq 7.0$, observed along the flat-slab shallowly dipping segment beneath Guerrero suggests that variations in fault geometry may play a key role in understanding the variability of slow slip dynamics (e.g (Brudzinski et al., 2016; Maury et al., 2018). Our numerical findings support the importance of 3D slab geometry in reproducing the spontaneous emergence of realistic SSE cycles. In our model, the velocity-weakening portion of the fault under near-lithostatic pore fluid pressure conditions (defined as W) is inversely correlated to the average dipping angle at specific depths (20–45 km). As a result, W varies significantly (between 60 and 160 km) along strike, as shown Figure 3b.

Previously modeled SSE source characteristics (e.g., recurrence, slip rate, cumulative slip, etc.,) roughly scale with W/h^* (Liu & Rice, 2009). In our preferred model, h^* is kept constant along the entire slab and the relatively large W is a dominant factor that leads to large magnitudes and long recurrence interval characterizing long-term SSE dynamics in Guerrero. We perform additional simulations, which confirm the effect of W assuming constant h^*. Increasing W by 6 km, which represents only a 4% increase with respect to its preferred value ($W = 144.4$ km), leads to a notable increase in the median periodicity, magnitude, and peak slip rate of the emerging SSEs (Figure S4). Thus, even small changes in W/h^* have an effect on the characteristics of modeled SSEs.

The lateral curvature of the slab influences the shear stress evolution on the fault. In previous models, larger SSEs tend to appear where the fault is flatter; and steepening of the slab promotes SSE arrest (Li & Liu, 2016). Here, we additionally find that the lateral patterns of the modeled SSEs, especially smaller events appearing on the western part of the fault, vary moderately over time; this can be seen by comparing the along-strike migration patterns of SSEs shown in Figure 3a and Figure S5. We note that this is a direct result of the complex evolution of shear stresses, since our simulation is independent of initial conditions after a short spin-up period (Rubin, 2008; Liu, 2014). This along-strike variation reflects an additional effect of the non-planar fault (Matsuzawa et al., 2013), as the western part of the fault has narrower W, which promotes more frequent and smaller SSEs (e.g., Liu & Rice, 2009). However, this influence on the lateral pattern is only moderate, as the termination of an individual modeled SSE is largely affected by the stress field left behind from previous events and is thus transient over time (Figure S5b).

4.2. Implications for Diverse Slow Slip Along Central Mexico

In our preferred SSE cycle model, smaller SSEs nucleate northwest of the GSG (Figure 3a). In contrast, no SSEs have been observed in this region (~101.5–103.5 W) between 2001 and 2014 (Maury et al., 2018). Recent time-dependent GPS modeling of the 2019 M_w 7.0 SSE resolved aseismic slip starting northwest of the GSG (Cruz-Atienza et al., 2021), implying that this region may host slow slip.

To assess whether the modeled Type III SSEs would be detected given current GPS noise thresholds (<5 mm) we calculate the synthetic surface displacement of several events (Figure S9). We find notable displacements of 10–25 mm at several close GPS stations. This inconsistency between observation and modeling may suggest that the region northwest of the GSG requires more complex frictional properties or pore pressure distribution than what our model assumes.

The emergence of SSEs also depends on the frictional properties and pore fluid pressure distribution on the plate interface, which in our model are assumed to be only depth-dependent. However, the heterogeneous distribution of the ultraslow velocity layer (USL) imaged atop the Cocos plate (Dougherty & Clayton, 2014; Song et al., 2009), implies that along-strike variations in pore fluid pressure exist beneath both the Guerrero and Oaxaca regions. Additionally, the degree of coupling of the plate interface, which also gives insight into the distribution of the frictional properties, also exhibits along-strike changes (Radiguet et al., 2012, 2016).

Our model does not include short-term SSEs associated with low-frequency earthquakes (LFEs) at the so-called sweet spot further down-dip (Frank et al., 2015; Husker et al., 2012), due to limited geodetic resolution by only two close continuous GPS stations (Figure 1). This along-dip variation of SSE recurrence may reflect the pore fluid increasing with depth modulated by temperature-dependent silica deposition as suggested by seismic imaging in northern Cascadia (Audet & Burgmann, 2014). Future application of our modeling approach may help to understand the along-dip variation in SSE source characteristics in future work.

Smaller and more frequent SSEs have been observed in Oaxaca (Graham et al., 2016), southeast of Guerrero (blue contours in Figure 1). The occurrence of these SSEs may be related to the narrower width of the USL in this region (Song et al., 2009), which results in a smaller W and thus in SSEs with lower magnitudes and shorter recurrence intervals (Figure S4). The convergence rate of the Cocos plate under the North American plate, which increases southeastwards (DeMets et al., 2010), may also contribute to the shorter recurrence period of SSEs in Oaxaca, as this factor has been shown to inversely correlate with the recurrence interval of simulated SSEs (Li et al., 2018; Shibazaki et al., 2012; Watkins et al., 2015).

4.3. Implications for Source Scaling Relation

Our scaling falls in between the $M \sim T^3$ scaling found for a wide range of regular earthquakes (Kanamori & Anderson, 1975) and the $M \sim T$ scaling inferred from a global compilation of SSEs (Ide et al., 2007). The differences in scaling relations between slow slip and regular earthquakes has been documented for many subduction zones (Ide et al., 2007; Gao et al., 2012; Peng & Gomberg, 2010) and is typically attributed to fundamental differences in the underlying physical mechanisms. For the four long-term SSEs inferred from geodetic inversion (Radiguet et al., 2012, 2016), the observational scaling remains difficult to constrain due to the insufficient range of magnitudes and durations (Figure 3e).

It has been shown that simultaneous SSEs tend to have a different scaling relation than temporally non-overlapping, distinct SSEs, regardless of fault geometry and friction properties (Liu, 2014). Future modeling is required to include smaller SSEs further downdip to understand the factors controlling the observed scaling of SSEs in Guerrero. For instance, Rousset et al. (2017) constrained the moment-duration scaling of smaller SSEs and long-term SSEs and find that the moment scales with the duration with a power of 1–2, with the exponent being closer to 2 when accounting for the loading and release periods of long-term SSEs.

Recently, a cubic moment-duration scaling has been reported for deep SSEs in the Nankai (Takagi et al., 2019), Cascadia (Michel et al., 2019) and Mexico (Frank & Brodsky, 2019) subduction zones from geodetic and seismic observations. We note that an apparent shift of the scaling from $M \sim T$ to $M \sim T^3$ may result from breaking a large slow slip event (as the 2006 SSE) into a cluster of daily slow transients calibrated by seismic LFE records (Frank & Brodsky, 2019). The identification based on cut-off slip rate may also considerably influence the geodetically resolved moment-duration scaling (Figure S7b) (Li & Liu, 2017). Our results suggest that the separation between the two scaling relations may be not distinct. Rather, dynamic variability of natural fault slip (Peng & Gomberg, 2010) may also reflect in, potentially regional specific, continuous variability in SSE scaling relations.

5. Conclusions

We present the first 3D sequence simulations of long-term slow slip events in the Guerrero Seismic Gap, Mexico. Our model accounts for a realistic 3D fault geometry and laboratory-derived rate-and-state friction, and assumes the presence of high-fluid pressure regions atop the subducting slab at SSE source depths, supported by the existence of ultralow velocity layer revealed by high-resolution seismic imaging. The simulation produces spontaneously emerging long-term SSEs under constant geological plate convergence.

Our preferred model successfully reproduces the main source characteristics of long-term SSEs along the flat-slab segment beneath Guerrero as well as surface deformation obtained from continuous GPS measurements. In particular, we find that the source characteristics of the simulated SSEs agree well with those of the long-term SSEs. Our model results suggest that the unusually large magnitudes ($M_w \geq 7.0$) and long recurrence intervals (~4 years) of SSEs in Guerrero are favored by the shallow-dipping flat-slab segment of the Cocos plate.

In addition, three distinct types of SSEs emerge in the model, which suggests that along-strike changes in the slab dip angle may affect the lateral distribution of SSEs. Modeled SSEs follow a moment-duration scaling of $M \sim T^{1.76}$, which is between the originally proposed linear scaling and the recently reported cubic relation for SSEs in Nankai, Cascadia and Mexico. Future work may be directed toward understanding the origin of the scaling trend of both long-term and short-term SSEs in Guerrero and Oaxaca, Mexico.

Data Availability Statement

The model parameter setup and simulation data is available at https://doi.org/10.5281/zenodo.4561753.

Acknowledgments
The work presented in this paper was supported by the European Research Council (ERC) under the European Union's Horizon 2020 research and innovation program (ERC Starting Grant TEAR agreement No. 852992), the German Research Foundation (DFG project grants no. GA 2465/2-1, GA 2465/3-1) and the Rutherford Discovery Fellowship from the Royal Society of New Zealand. Computing resources were provided by the Institute of Geophysics of LMU Munich (Oeser et al., 2006), the Leibniz Supercomputing Center (LRZ, projects no. pr63qo and pr45fi on SuperMUC), and the New Zealand eScience Infrastructure (NeSI) high-performance computing facilities. The authors thank Dr. Mathilde Radiguet for kindly sharing the GPS inversion results of the Guerrero slow slip events. The authors appreciate the fruitful discussions with Luis A. Dalguer and the Seismology group at Munich University (LMU). We thank Editor Germán Prieto and two anonymous reviewers for their comments that helped us improve the manuscript. DL initialized the project and created the mesh file. AP performed all simulations and created figures under the supervision of DL and AG. All authors contributed to the discussion of the results and writing of the manuscript.

References

Audet, P., Bostock, M. G., Christensen, N. I., & Peacock, S. M. (2009). Seismic evidence for overpressured subducted oceanic crust and megathrust fault sealing. *Nature*, *457*, 76–78. https://doi.org/10.1038/nature07650

Audet, P., & Burgmann, R. (2014). Possible control of subduction zone slow-earthquake periodicity by silica enrichment. *Nature*, *510*, 389–392. https://doi.org/10.1038/nature13391

Barbot, S. (2019). Slow-slip, slow earthquakes, period-two cycles, full and partial ruptures, and deterministic chaos in a single asperity fault. *Tectonophysics*, *768*, 228171. https://doi.org/10.1016/j.tecto.2019.228171

Brudzinski, M. R., Schlanser, K. M., Kelly, N. J., DeMets, C., Grand, S. P., Márquez-Azúa, B., & Cabral-Cano, E. (2016). Tectonic tremor and slow slip along the northwestern section of the Mexico subduction zone. *Earth and Planetary Science Letters*, *454*, 259–271. https://doi.org/10.1111/j.1365-246X.2007.03542.x

Cruz-Atienza, V. M., Tago, J., Villafuerte, C., Wei, M., Garza-Girón, R., Dominguez, L. A., et al. (2021). Short-term interaction between silent and devastating earthquakes in Mexico. *Nature Communications*, *12*. 2171. https://doi.org/10.1038/s41467-021-22326-6

DeMets, C., Gordon, R. G., & Argus, D. F. (2010). Geologically current plate motions. *Geophysical Journal International*, *181*(1), 1–80. https://doi.org/10.1111/j.1365-246X.2009.04491.x

Dougherty, S. L., & Clayton, R. W. (2014). Seismicity and structure in central Mexico: Evidence for a possible slab tear in the South Cocos plate. *Journal of Geophysical Research: Solid Earth*, *119*(4), 3424–3447. https://doi.org/10.1002/2013jb010883

Dragert, H., Wang, K., & James, T. S. (2001). A silent slip event on the deeper Cascadia subduction interface. *Science*, *292*(5521), 1525–1528. https://doi.org/10.1126/science.1060152

Fasola, S., Brudzinski, M. R., Ghouse, N., Solada, K., Sit, S., Cabral-Cano, E., et al. (2016). New perspective on the transition from flat to steeper subduction in Oaxaca, Mexico, based on seismicity, nonvolcanic tremor, and slow slip. *Journal of Geophysical Research: Solid Earth*, *121*(3), 1835–1848. https://doi.org/10.1002/2015JB012709

Frank, W. B., & Brodsky, E. E. (2019). Daily measurement of slow slip from low-frequency earthquakes is consistent with ordinary earthquake scaling. *Science Advances*, *5*(10), eaaw9386. https://doi.org/10.1126/sciadv.aaw9386

Frank, W. B., Radiguet, M., Rousset, B., Shapiro, N., Husker, A., Kostoglodov, V., et al. (2015). Uncovering the geodetic signature of silent slip through repeating earthquakes. *Geophysical Research Letters*, *42*, 2774–2779. https://doi.org/10.1002/2015gl063685

Fu, Y., Liu, Z., & Freymueller, J. T. (2015). Spatiotemporal variations of the slow slip event between 2008 and 2013 in the southcentral Alaska subduction zone. *Geochemistry, Geophysics, Geosystems*, *16*(7), 2450–2461. https://doi.org/10.1002/2015GC005904

Gao, H., Schmidt, D. A., & Weldon, R. J. (2012). Scaling relationships of source parameters for slow slip events. *Bulletin of the Seismological Society of America*, *102*(1), 352–360. https://doi.org/10.1785/0120110096

Graham, S., DeMets, C., Cabral-Cano, E., Kostoglodov, V., Rousset, B., Walpersdorf, A., et al. (2016). Slow slip history for the MEXICO subduction zone: 2005 Through 2011. *Pure and Applied Geophysics*, *173*, 3445–3465. https://doi.org/10.1007/s00024-015-1211-x

Gualandi, A., Perfettini, H., Radiguet, M., Cotte, N., & Kostoglodov, V. (2017). GPS deformation related to the M_w7.3, 2014, Papanoa earthquake (Mexico) reveals the aseismic behavior of the Guerrero seismic gap. *Geophysical Research Letters*, *44*(12), 6039–6047. https://doi.org/10.1002/2017gl072913

He, C., Wang, Z., & Yao, W. (2007). Frictional sliding of gabbro gouge under hydrothermal conditions. *Tectonophysics*, *445*, 353–362. https://doi.org/10.1016/j.tecto.2007.09.008

Husker, A., & Davis, P. M. (2009). Tomography and thermal state of the Cocos plate subduction beneath Mexico City. *Journal of Geophysical Research: Solid Earth*, *114*, B04306. https://doi.org/10.1029/2008JB006039

Husker, A., Frank, W. B., Gonzalez, G., Avila, L., Kostoglodov, V., & Kazachkina, E. (2019). Characteristic tectonic tremor activity observed over multiple slow slip cycles in the Mexican subduction zone. *Journal of Geophysical Research: Solid Earth*, *124*(1), 599–608. https://doi.org/10.1029/2018JB016517

Husker, A. L., Kostoglodov, V., Cruz-Atienza, V. M., Legrand, D., Shapiro, N. M., Payero, J. S., et al. (2012). Temporal variations of non-volcanic tremor (NVT) locations in the Mexican subduction zone: Finding the NVT sweet spot. *Geochemistry, Geophysics, Geosystems*, *13*(3). https://doi.org/10.1029/2011gc003916

Hyndman, R. D. (2013). Downdip landward limit of Cascadia great earthquake rupture. *Journal of Geophysical Research: Solid Earth*, *118*(10), 5530–5549. https://doi.org/10.1002/jgrb.50390

Ide, S., Beroza, G. C., Shelly, D. R., & Uchide, T. (2007). A scaling law for slow earthquakes. *Nature*, *447*(7140), 76–79. https://doi.org/10.1038/nature05780

Jödicke, H., Jording, A., Ferrari, L., Arzate, J., Mezger, K., & Rüpke, L. (2006). Fluid release from the subducted Cocos plate and partial melting of the crust deduced from magnetotelluric studies in southern Mexico: Implications for the generation of volcanism and subduction dynamics. *Journal of Geophysical Research: Solid Earth*, *111*, B08102. https://doi.org/10.1029/2005JB003739

Kanamori, H., & Anderson, D. L. (1975). Theoretical basis of some empirical relations in seismology. *Bulletin of the Seismological Society of America*, *65*(5), 1073–1095. https://doi.org/10.1002/2014JB011144

Kim, Y., Clayton, R. W., & Jackson, J. M. (2010). Geometry and seismic properties of the subducting Cocos plate in central Mexico. *Journal of Geophysical Research: Solid Earth*, *115*, B06310. https://doi.org/10.1029/2009JB006942

Kostoglodov, V., Singh, S. K., Santiago, J. A., Franco, S. I., Larson, K. M., Lowry, A. R., & Bilham, R. (2003). A large silent earthquake in the Guerrero seismic gap, Mexico. *Geophysical Research Letters*, *30*(15), 1807. https://doi.org/10.1029/2003GL017219

Li, D., & Liu, Y. (2016). Spatiotemporal evolution of slow slip events in a nonplanar fault model for northern Cascadia subduction zone. *Journal of Geophysical Research: Solid Earth*, *121*(9), 6828–6845. https://doi.org/10.1002/2016JB012857

Li, D., & Liu, Y. (2017). Modeling slow-slip segmentation in Cascadia subduction zone constrained by tremor locations and gravity anomalies. *Journal of Geophysical Research: Solid Earth*, *122*(4), 3138–3157. https://doi.org/10.1002/2016JB013778

Li, H., Wei, M., Li, D., Liu, Y., Kim, Y., & Zhou, S. (2018). Segmentation of slow slip events in south central Alaska possibly controlled by a subducted oceanic plateau. *Journal of Geophysical Research: Solid Earth*, *123*(1), 418–436. https://doi.org/10.1002/2017JB014911

Liu, Y. (2014). Source scaling relations and along-strike segmentation of slow slip events in a 3-D subduction fault model. *Journal of Geophysical Research: Solid Earth*, *119*(8), 6512–6533. https://doi.org/10.1002/2014JB011144

Liu, Y., & Rice, J. R. (2005). Aseismic slip transients emerge spontaneously in three-dimensional rate and state modeling of subduction earthquake sequences. *Journal of Geophysical Research: Solid Earth*, *110*, B08307. https://doi.org/10.1029/2004JB003424

Liu, Y., & Rice, J. R. (2007). Spontaneous and triggered aseismic deformation transients in a subduction fault model. *Journal of Geophysical Research: Solid Earth*, *112*, B09404. https://doi.org/10.1029/2007JB004930

Liu, Y., & Rice, J. R. (2009). Slow slip predictions based on granite and gabbro friction data compared to GPS measurements in northern Cascadia. *Journal of Geophysical Research: Solid Earth*, *114*, B09407. https://doi.org/10.1029/2008JB006142

Liu, Z., Owen, S., Dong, D., Lundgren, P., Webb, F., Hetland, E., & Simons, M. (2010). Integration of transient strain events with models of plate coupling and areas of great earthquakes in southwest Japan. *Geophysical Journal International*, *181*(3), 1292–1312. https://doi.org/10.1111/j.1365-246X.2010.04599.x

Lowry, A. R., Larson, K. M., Kostoglodov, V., & Bilham, R. (2001). Transient fault slip in Guerrero, southern Mexico. *Geophysical Research Letters*, *28*(19), 3753–3756. https://doi.org/10.1029/2001GL013238

Manea, V. C., & Manea, M. (2011). Flat-Slab Thermal Structure and Evolution Beneath Central Mexico. *Pure and Applied Geophysics*, *168*(8), 1475–1487. https://doi.org/10.1007/s00024-010-0207-9

MASE (2007). *Meso America subduction experiment*. Caltech. Dataset.

Matsuzawa, T., Shibazaki, B., Hirose, H., & Hirose, H. (2013). Comprehensive model of short- and long-term slow slip events in the Shikoku region of Japan, incorporating a realistic plate configuration. *Geophysical Research Letters*, *40*(19), 5125–5130. https://doi.org/10.1002/grl.51006

Maury, J., Ide, S., Cruz-Atienza, V. M., & Kostoglodov, V. (2018). Spatiotemporal variations in slow earthquakes along the Mexican subduction zone. *Journal of Geophysical Research: Solid Earth*, *123*(2), 1559–1575. https://doi.org/10.1002/2017JB014690

McLaskey, G. C., & Yamashita, F. (2017). Slow and fast ruptures on a laboratory fault controlled by loading characteristics. *Journal of Geophysical Research: Solid Earth*, *122*(5), 3719–3738. https://doi.org/10.1002/2016JB013681

Meade, B. J. (2007). Algorithms for the calculation of exact displacements, strains, and stresses for triangular dislocation elements in a uniform elastic half space. *Computers & Geosciences*, *33*(8), 1064–1075. https://doi.org/10.1016/j.cageo.2006.12.003

Michel, S., Gualandi, A., & Avouac, J.-P. (2019). Similar scaling laws for earthquakes and Cascadia slow-slip events. *Nature*, *574*(7779), 522–526. https://doi.org/10.1038/s41586-019-1673-6

Oeser, J., Bunge, H.-P., & Mohr, M. (2006). Cluster design in the earth sciences tethys. *International conference on high performance computing and communications* (pp. 31–40). https://doi.org/10.1007/11847366_4

Peng, Z., & Gomberg, J. (2010). An integrated perspective of the continuum between earthquakes and slow-slip phenomena. *Nature Geoscience*, *3*, 599–607. https://doi.org/10.1038/ngeo940

Pérez-Campos, X., Kim, Y., Husker, A., Davis, P. M., Clayton, R. W., Iglesias, A., et al. (2008). Horizontal subduction and truncation of the Cocos Plate beneath central Mexico. *Geophysical Research Letters*, *35*, L18303. https://doi.org/10.1029/2008GL035127

Radiguet, M., Cotton, F., Vergnolle, M., Campillo, M., Valette, B., Kostoglodov, V., & Cotte, N. (2011). Spatial and temporal evolution of a long term slow slip event: The 2006 Guerrero slow slip event. *Geophysical Journal International*, *184*(2), 816–828. https://doi.org/10.1111/j.1365-246X.2010.04866.x

Radiguet, M., Cotton, F., Vergnolle, M., Campillo, M., Walpersdorf, A., Cotte, N., & Kostoglodov, V. (2012). Slow slip events and strain accumulation in the Guerrero gap, Mexico. *Journal of Geophysical Research: Solid Earth*, *117*, B04305n. https://doi.org/10.1029/2011JB008801

Radiguet, M., Perfettini, H., Cotte, N., Gualandi, A., Valette, B., Kostoglodov, V., et al. (2016). Triggering of the 2014 M_w 7.3 Papanoa earthquake by a slow slip event in Guerrero, Mexico. *Nature Geoscience*, *9*(11), 829–833. https://doi.org/10.1038/ngeo2817

Rice, J. R. (1993). Spatiotemporal complexity of slip on a fault. *Journal of Geophysical Research*, *98*(B6), 9885–9907. https://doi.org/10.1029/93JB00191

Rousset, B., Campillo, M., Lasserre, C., Frank, W. B., Cotte, N., Walpersdorf, A., et al. (2017). A geodetic matched filter search for slow slip with application to the Mexico subduction zone. *Journal of Geophysical Research: Solid Earth*, *122*(12), 10. https://doi.org/10.1002/2017JB014448

Rubin, A. M. (2008). Episodic slow slip events and rate-and-state friction. *Journal of Geophysical Research*, *113*, B11414. https://doi.org/10.1029/2008jb005642

Rubin, A. M., & Ampuero, J.-P. (2005). Earthquake nucleation on (aging) rate and state faults. *Journal of Geophysical Research: Solid Earth*, *110*, B11312. https://doi.org/10.1029/2005JB003686

Rudolf-Navarro, A. H., Muñoz-Diosdado, A., & Angulo-Brown, F. (2010). Seismic quiescence patterns as possible precursors of great earthquakes in mexico. *International Journal of the Physical Sciences*, *5*(6), 651–670. https://doi.org/10.5897/IJPS.9000492

Saffer, D. M., & Wallace, L. M. (2015). The frictional, hydrologic, metamorphic and thermal habitat of shallow slow earthquakes. *Nature Geoscience*, *8*(8), 594–600. https://doi.org/10.1038/ngeo2490

Scholz, C. H. (1998). Earthquakes and friction laws. *Nature*, *391*(6662), 37–42. https://doi.org/10.1038/34097

Schwartz, S. Y., & Rokosky, J. M. (2007). Slow slip events and seismic tremor at circum-Pacific subduction zones. *Reviews of Geophysics*, *45*, RG3004. https://doi.org/10.1029/2006RG000208

Shibazaki, B., Obara, K., Matsuzawa, T., & Hirose, H. (2012). Modeling of slow slip events along the deep subduction zone in the Kii Peninsula and Tokai regions, southwest Japan. *Journal of Geophysical Research: Solid Earth*, *117*, B06311. https://doi.org/10.1029/2011JB009083

Shibazaki, B., Wallace, L. M., Kaneko, Y., Hamling, I., Ito, Y., & Matsuzawa, T. (2019). Three-dimensional modeling of spontaneous and triggered slow-slip events at the Hikurangi subduction zone, New Zealand. *Journal of Geophysical Research: Solid Earth*, *124*(12), 13250–13268. https://doi.org/10.1029/2019JB018190

Song, T. R., Helmberger, D. V., Brudzinski, M. R., Clayton, R. W., Davis, P., Perez-Campos, X., & Singh, S. K. (2009). Subducting slab ultra-slow velocity layer coincident with silent earthquakes in southern Mexico. *Science*, *324*(5926), 502–506. https://doi.org/10.1126/science.1167595

Takagi, R., Uchida, N., & Obara, K. (2019). Along-strike variation and migration of long-term slow slip events in the western Nankai subduction zone, Japan. *Journal of Geophysical Research: Solid Earth*, *124*(4), 3853–3880. https://doi.org/10.1029/2018JB016738

Vergnolle, M., Walpersdorf, A., Kostoglodov, V., Tregoning, P., Santiago, J. A., Cotte, N., & Franco, S. I. (2010). Slow slip events in Mexico revised from the processing of 11 year GPS observations. *Journal of Geophysical Research*, *115*, B08403. https://doi.org/10.1029/2009JB006852

Villafuerte, C., & Cruz-Atienza, V. M. (2017). Insights into the causal relationship between slow slip and tectonic tremor in Guerrero, Mexico. *Journal of Geophysical Research: Solid Earth*, *122*(8), 6642–6656. https://doi.org/10.1002/2017JB014037

Wallace, L. M., & Beavan, J. (2010). Diverse slow slip behavior at the Hikurangi subduction margin, New Zealand. *Journal of Geophysical Research: Solid Earth*, *115*, B12402. https://doi.org/10.1029/2010JB007717

Watkins, W. D., Colella, H. V., Brudzinski, M. R., Richards-Dinger, K. B., & Dieterich, J. H. (2015). The role of effective normal stress, frictional properties, and convergence rates in characteristics of simulated slow slip events. *Geophysical Research Letters*, *42*(4), 1061–1067. https://doi.org/10.1002/2014GL062794

Wech, A. G., & Creager, K. C. (2011). A continuum of stress, strength and slip in the Cascadia subduction zone. *Nature Geoscience*, *4*(9), 624–628. https://doi.org/10.1038/ngeo1215

Wei, M., Kaneko, Y., Liu, Y., & McGuire, J. J. (2013). Episodic fault creep events in California controlled by shallow frictional heterogeneity. *Nature Geoscience*, *6*, 566–570. https://doi.org/10.1038/ngeo1835

Wei, M., Kaneko, Y., Shi, P., & Liu, Y. (2018). Numerical modeling of dynamically triggered shallow slow slip events in New Zealand by the 2016 Mw 7.8 Kaikoura earthquake. *Geophysical Research Letters*, *45*(10), 4764–4772. https://doi.org/10.1029/2018GL077879

References From the Supporting Information

Dieterich, J. (1979). Modeling of rock friction 1. Experimental results and constitutive equations. *Journal of Geophysical Research: Solid Earth*, *84*(B5), 2161–2168. https://doi.org/10.1029/JB084iB05p02161

Dieterich, J. (2007). Applications of rate-and state-dependent friction to models of fault-slip and earthquake occurrence. *Treatise on Geophysics*, *4*, 107–129. https://doi.org/10.1016/B978-044452748-6.00065-1

Ruina, A. L. (1983). Slip instability and state variable friction laws. *Journal of Geophysical Research: Solid Earth*, *88*(B12), 10359–10370. https://doi.org/10.1029/JB088iB12p10359

Walpersdorf, A., Cotte, N., Kostoglodov, V., Vergnolle, M., Radiguet, M., Santiago, J. A., & Campillo, M. (2011). Two successive slow slip events evidenced in 2009–2010 by a dense GPS network in Guerrero, Mexico. *Geophysical Research Letters*, *38*(15). https://doi.org/10.1029/2011GL048124

Supporting Information for "3D modeling of long-term slow slip events along the flat-slab segment in the Guerrero Seismic Gap, Mexico"

Andrea Perez-Silva[1,*], Duo Li[1], Alice-Agnes Gabriel[1], Yoshihiro Kaneko[2]

[1]Department of Earth and Environmental Sciences, Ludwig-Maximilians-University Munich.

[2]Department of Geophysics, Graduate School of Science, Kyoto University, Japan

[*]Now at Victoria University of Wellington, School of Geography, Environment and Earth Sciences, New Zealand.

Contents of this file

Additional Supporting Information (Files uploaded separately)

1. Movie S1-S4

Introduction

The supporting information includes a brief description of the governing equations implemented in the simulation code developed by Li and Liu (2016) (Text S1), parameter exploration of W and h^* (Text S2), an alternative model setup with no velocity-strengthening bands (Text S3), source characteristics of four SSE episodes inferred from geodetic inversion (Table S1), supporting figures of simulation results (Figure S1-S9), and movies showing the spatial and temporal evolution of the slip rate on the fault during four SSE episodes (Movie S1-S4).

Text S1: Governing equations

We use the code developed by Li and Liu (2016), where a non-planar fault is embedded in an elastic half-space Earth. This model implements a quasi-dynamic approach, as defined by Rice (1993), which relates shear traction and fault slip as follows (discretized in space and time):

$$\tau_i(t) = -\sum_{j=1}^{N} K_{ij} \left(\delta_j(t) - V_{pl}t\right) - \eta \frac{d\delta_i(t)}{dt}, \tag{1}$$

where t is the time step and the subscripts i, j indicate elements in space. τ_i and δ_i are shear stress and slip at element i, respectively. The stiffness matrix or Green's function, K_{ij}, describes the change in shear stress in element i due to a unit dislocation in the dip direction at element j. V_{pl} is the plate convergence rate, that we take from the relative plate motion model PVEL (DeMets et al., 2010). η is the radiation damping factor, defined as $\eta = \mu/2c_s$, where μ is the elastic shear modulus and c_s is the shear wave speed. This term reflects a part of elastodynamic instantaneous change in $\tau_i(t)$ due to the $d\delta_i/dt$.

We incorporate the laboratory-derived rate-and state-dependent friction law (Ruina, 1983; Dieterich, 1979, 2007) to constrain yielding and slip on the prescribed slab interface. The shear strength of the fault, τ, depends logarithmically on the slip rate V and a state variable θ, which can be interpreted as the temporal evolution of the state of asperity contacts (Dieterich, 1979; Ruina, 1983), as

$$\tau = \bar{\sigma} f = \bar{\sigma} \left[f_0 + a \ln \left(\frac{V}{V_0} \right) + b \ln \left(\frac{V_0 \theta}{d_c} \right) \right], \tag{2}$$

where f is the friction coefficient, f_0 is the steady state friction coefficient at reference slip rate V_0, d_c is the critical slip distance over which a fault loses or regains its frictional strength after a perturbation in the loading conditions and a and b are dimensionless constitutive parameters. For $a-b>0$, the interface is steady state velocity-strengthening and slip is stable. For $a-b<0$, the sliding surface is steady state velocity-weakening and unstable slip is possible. The effective normal stress ($\bar{\sigma}$) is defined as the difference between the lithostatic normal stress (σ_n) and the pore fluid pressure (p_f), with $\bar{\sigma} = \sigma_n(1-\lambda_p)$ and $\lambda_p = p_f/\sigma_n$.

In this study, the temporal evolution of the state variable is described by the 'aging' law, which assumes that the state variable θ increases monotonously with time for stationary contacts as supported by lab experiments (Dieterich, 1979):

$$\frac{d\theta}{dt} = 1 - \frac{V\theta}{d_c}. \tag{3}$$

The corresponding, upper-limit of critical nucleation size (h^*) is defined from the fracture energy balance for an expanding crack (Rubin & Ampuero, 2005), as

$$h^* = \frac{2\mu b d_c}{\pi(1-\nu)\overline{\sigma}(b-a)^2}, \tag{4}$$

where we assume shear modulus $\mu = 30$ GPa and Poisson ratio $\nu = 0.25$.

Text S2: Parameter sensitivity

We test the sensitivity of our simulated source characteristics to W and h^*. h^* depends on d_c as shown in Equation 4. To explore the parameter space of W/h^*, we perform two sets of simulations. In the first set, we fix $W = 144.44$ km and vary h^*= 150, 140, 130 and 122 km (Figure S3). In the second set, we fix h^*=122 km and change W. To vary W, we assume a different updip limit of the SSE zone, namely 22 km, 21 km and 20 km, which correspond to $W = 138.3$, 142 and 144.4 km, respectively. The downdip limit of the SSE zone is fixed at 45 km depth in all simulation cases. All other parameters are kept the same as in the main text. Note that the reported value of W was calculated at along-strike distance y = -98.3 km, which is approx. at the center (along-strike) of the GSG. For each simulation case, we report the maximum slip rate, recurrence interval and magnitudes of modeled SSEs between 5 and 50 years. We calculate the median, the 25th and 75th percentile of the distribution of each variable, respectively.

Figures S3 and S4 show the source characteristics of all emerging SSEs with respect to W/h^*. Simulations with lower W/h^* result in lower moment magnitudes and peak slip rates (Figures S3 and S4), whereas the median recurrence interval decreases when decreasing W/h^* (Figure S4).

Text S3: Alternative model setup

Here we show the results of an alternative model setup with no velocity-strengthening bands at the ends of fault. Our results, shown in Figure S8, indicate that the slip rate evolution does not change significantly regardless of the absence of velocity-strengthening

bands at the model domain edges. Most of the SSEs (red contours in Figure S8) extend up to -150 km to the south east (Y-axis in Figure S8). Only one event starts at Y < -200 km (see year 80 in Figure S8b). Even though the slip rate evolution is not exactly the same as in the preferred model (especially in the last 50 years, Figure S8b), the tendency of larger SSEs concentrating most of the slip on the western part of the fault persists. Most of the longest SSEs along-strike reach their highest slip rates on the eastern part of the fault (pointsxx where yellow arrows converge in Figure S8), which implies that most of the slip accumulates in this region. SSEs with the shortest along-strike extent emerge in the western part of the fault (green arrows in Figure S8), as in the preferred model.

Table S1. Main source characteristics of SSEs inferred from geodetic inversion.

Start year	Duration (months)	Moment magnitude (M_w)	Max. slip (cm)	References
2001	9	7.65	20	Radiguet et al. (2012) Graham et al. (2016)
2006	∼8	7.49 (7.3)[a]	20 (27)	Radiguet et al. (2012) Graham et al. (2016)
2010	12	7.53 (7.4)	20 (28)	Radiguet et al. (2012) Graham et al. (2016)
2014	∼11	7.6	25	Radiguet et al. (2016)

[a] Values in parentheses are results from Graham et al. (2016) only.

Movie S1-S4. The movies show the slip rate evolution on the fault during the four modeled SSEs that better fitted the characteristics of the 2001/2002, 2006, 2009/2010 and 2014 long-term SSEs in Guerrero, respectively. The distribution of the slip rate is shown in a logarithmic scale ($\log_{10}$ V) in m/s and the simulation time is shown on the top. The modeled SSEs follow a similar evolution pattern, which starts with the nucleation of two slip patches at the along-strike edges of the fault and continues with the migration of two slip fronts toward each other until they coalesce in a velocity peak ($V_{max} \sim 10^{-5.5}$ m/s). Afterwards, the slip fronts propagate bilaterally both along-strike and along-dip.

As a representative model of the 2010 SSE (Movie S3) we select a SSE that involves Type II and III events occurring close to each other in space and time, as described in section 3.1. These (almost) synchronous events may resemble the two high slip regions inferred geodetically (Walpersdorf et al., 2011; Radiguet et al., 2012; Graham et al., 2016).

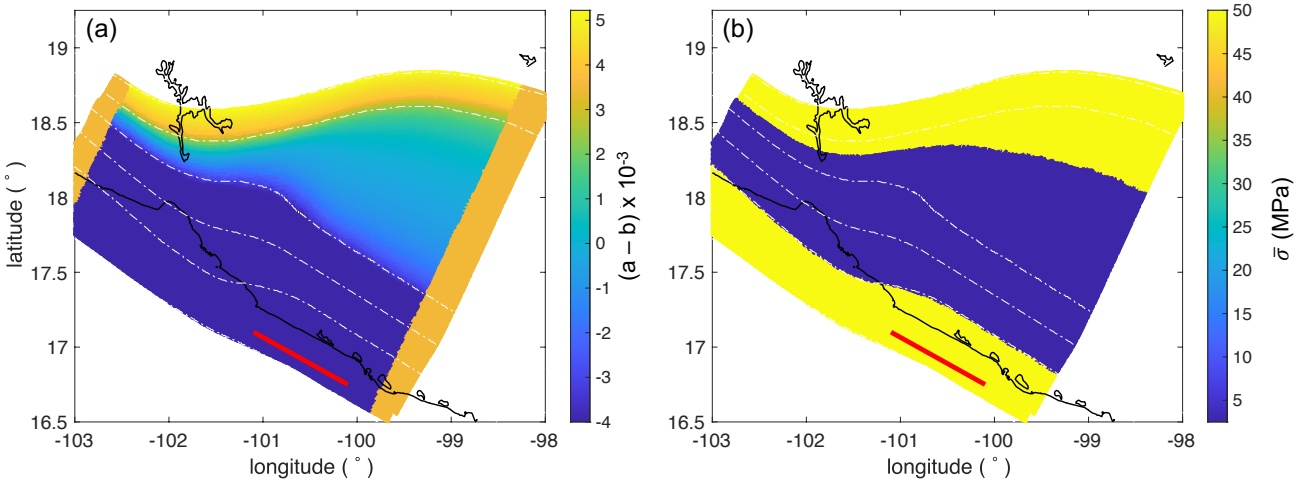

Figure S1. (a) Map view of friction parameter $(a - b)$ on the slab. Velocity-weakening region $(a - b < 0)$ extends from 10 - 45 km depth. (b) Map view of effective normal stress $(\bar{\sigma})$ on the slab. SSE zone extends from 20 to 45 km depth. Thick red line highlights western segment of Guerrero Seismic Gap. Dashed white lines show the depth contours from 20 to 60 km depth at 10-km spacing. Parameter distribution corresponds to the preferred model.

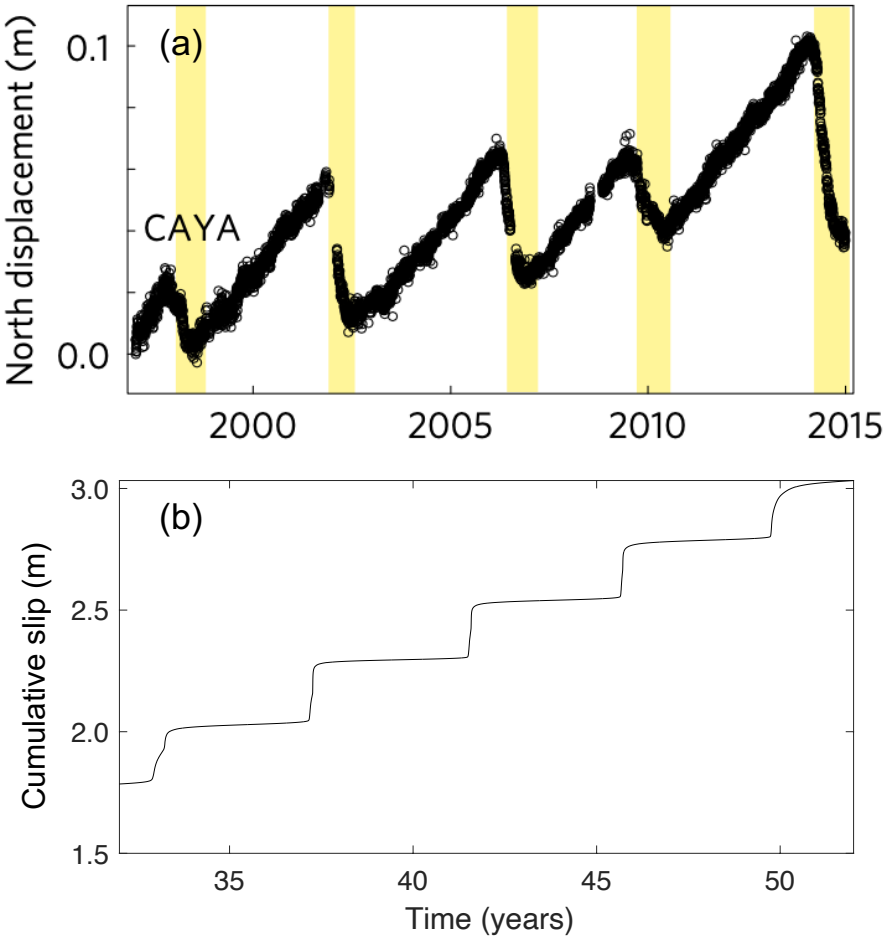

Figure S2. (a) Detrended North-component of displacement at station CAYA from 1998 to 2015. The yellow stripes highlight the occurrence of SSEs in 1998, 2001/2002, 2006, 2009/2010 and 2014. Figure taken from Radiguet et al. (2016), Fig. 1b. (b) Cumulative slip (in m) of the best-fitted model at the location of station CAYA projected on the model geometry.

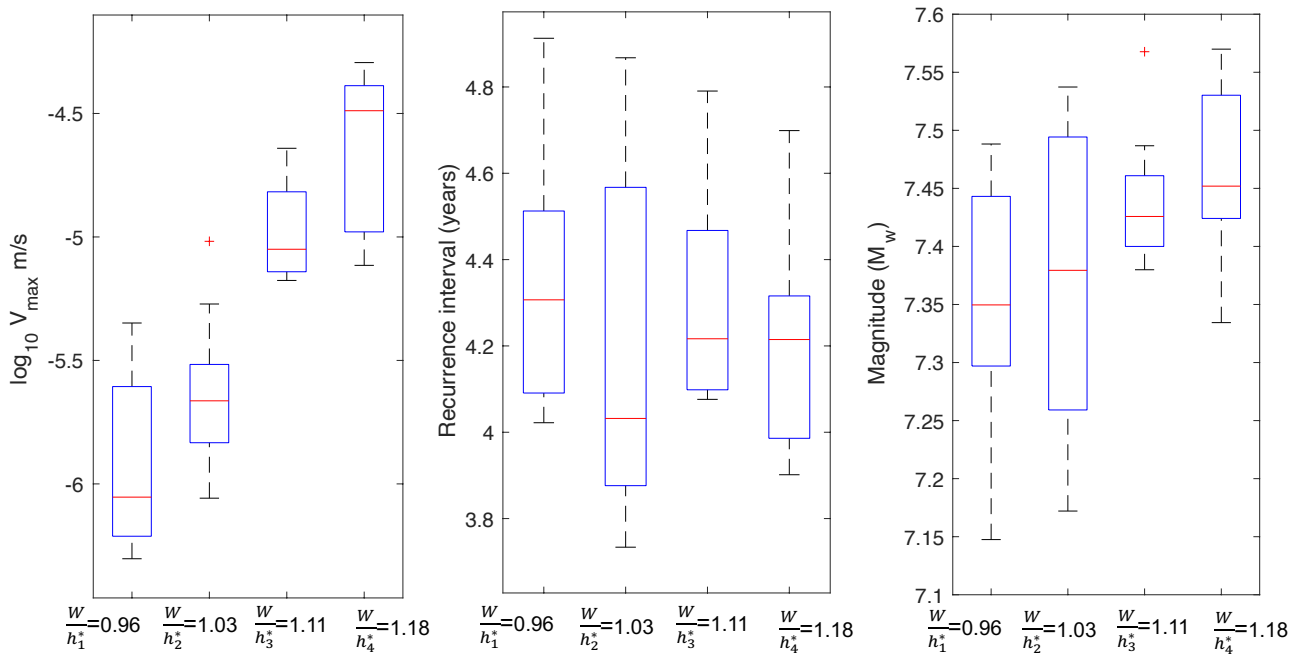

Figure S3. Box plot distribution of source parameters of SSEs with respect to W/h^*. Bottom and top edges of the blue box are the 25th and 75th percentile, respectively; red line, median; dashed lines, whiskers which cover 99.3 % of the data and red crosses are the outliers. Simulation cases with constant $\bar{\sigma}$=2.5 MPa, $W = 144.4$ km and variable h^*. $h_1^* = 150$ km, $h_2^* = 140$ km, $h_3^* = 130$ km and $h_4^* = 122$ km. Data taken from SSEs that emerged between 5 to 50 simulation years. When more that one SSE occurred along-strike, only the largest one is used to calculate the source parameters. The preferred model shown in the main text corresponds to the simulation case with $W/h^* = 1.18$. Source properties were calculated as described in section 3.2. Simulation cases with $W/h^* > 1.18$ (e.g. 1.23 for $h^* = 117$ km) lead to a seismic event in the first 15 years.

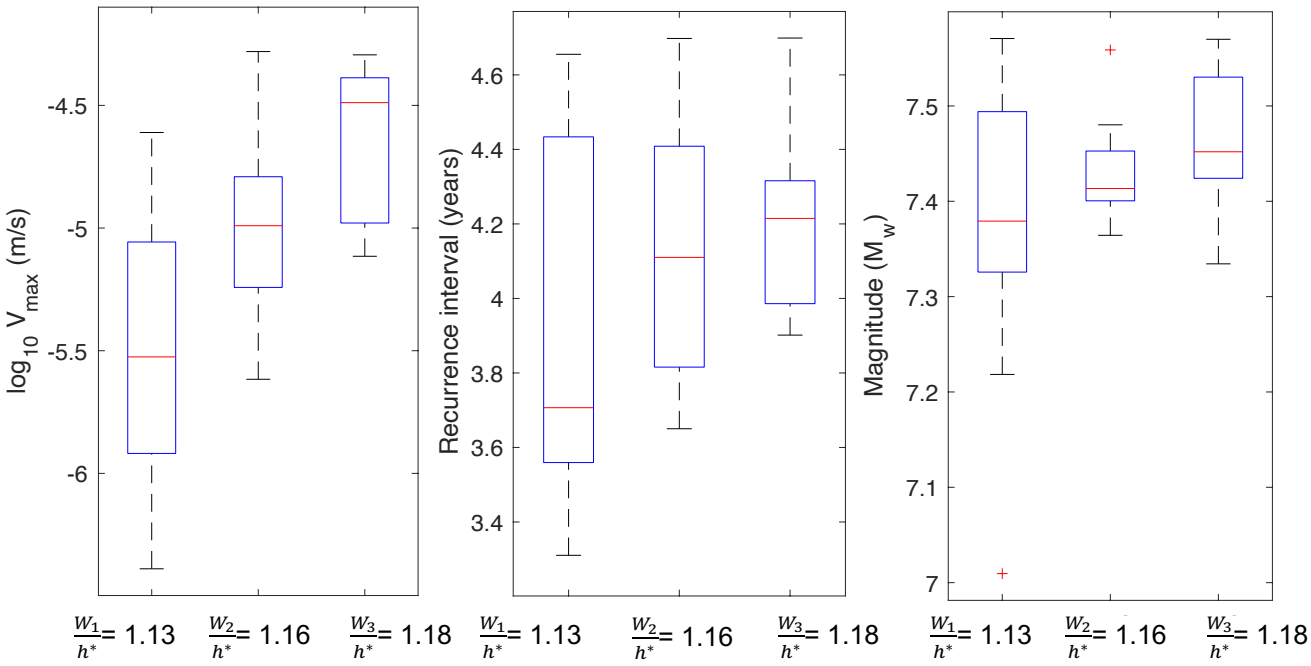

Figure S4. Same as Figure S3 except for $h^* = 122$ km and variable W. $W_1 = 138.3$ km, $W_2 = 142$ km, $W_3 = 144.4$ km; each value corresponds to different depth ranges of the SSE zone: 22 - 45 km, 21 - 45 km and 20 - 45 km, respectively. The preferred model shown in the main text corresponds to the simulation case with $W/h^* = 1.18$. Simulation cases with $W/h^* > 1.18$ (e.g. 1.22 for $W = 148.9$ km corresponding to an SSE zone from 19 to 45 km depth) lead to a seismic event in the first 15 years.

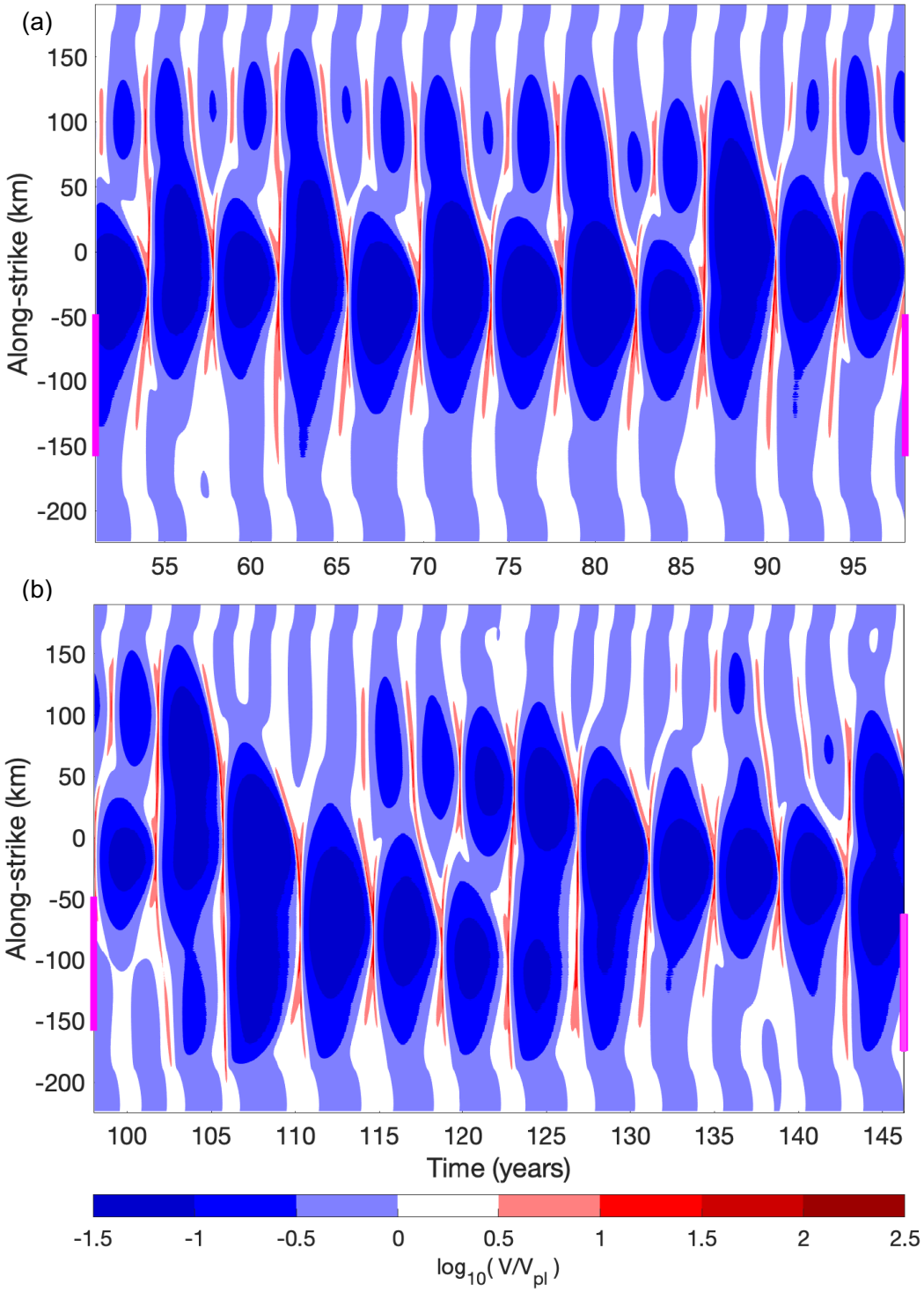

Figure S5. Spatial and temporal evolution of slip rate in $\log_{10}\mathrm{V/V}_{pl}$ at 30 km depth between year > 50 and ~ 145 of simulation time. Thick magenta lines indicate along-strike location of the Guerrero Seismic Gap. Results correspond to the preferred model, described in the main text.

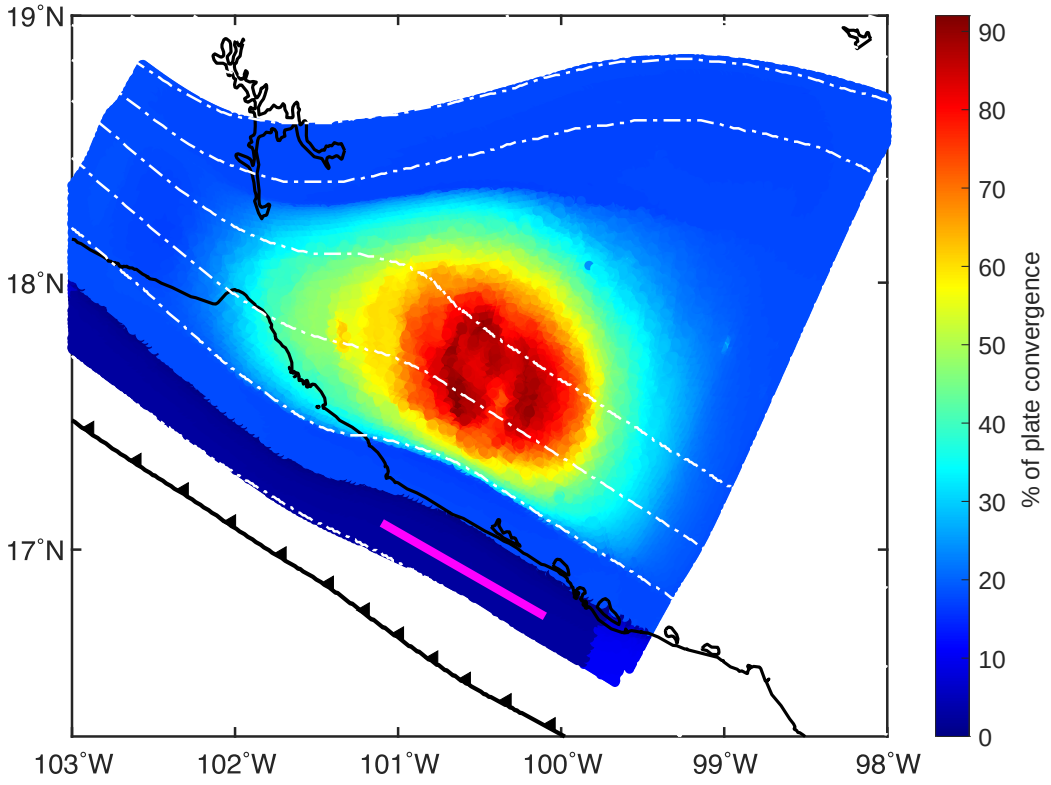

Figure S6. Slip released by long-term SSEs over 40 years as a percentage of total plate convergence. The dashed white line outlines the depth contours from 20 to 60 km depth. The magenta line highlights the location of the GSG. Results correspond to the preferred model, described in the main text.

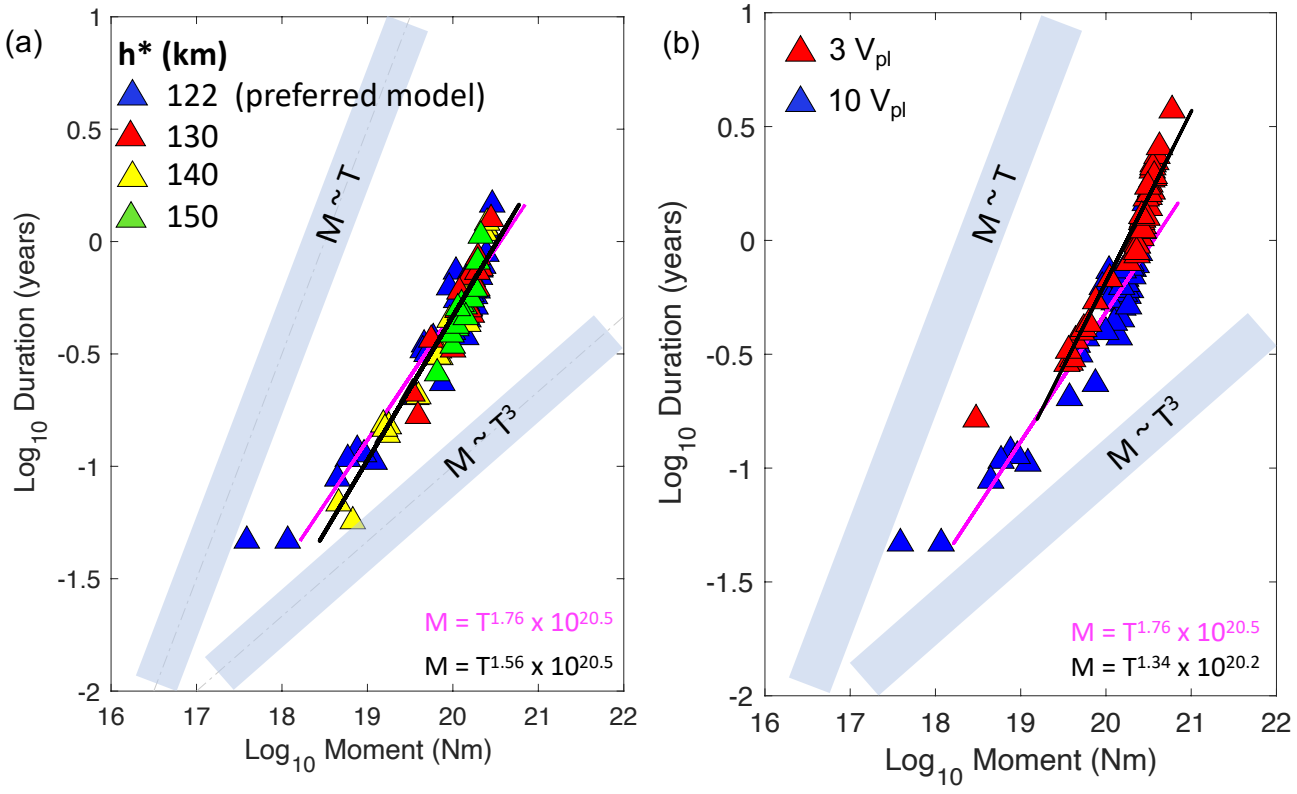

Figure S7. (a) Moment-duration scaling relation assuming a slip velocity threshold of 10 V_{pl} for simulation cases with different h^* (shown in color-coded triangles). $\bar{\sigma}$ = 2.5 MPa and W=144.4 km for all simulation cases. Simulation case with h^* = 122 km corresponds to the presented model in main text. Black thick line indicates best fit scaling for all simulations, $M = T^{1.56}$ x $10^{20.5}$. Magenta line shows the best fit scaling of the preferred model, $M = T^{1.76}$ x $10^{20.5}$. Scaling trends of M $\sim$ T and M $\sim$ T^3 are shown for comparison. (b) Moment-duration scaling for preferred model assuming two slip velocity thresholds: 3 V_{pl} (red triangles) and 10 V_{pl} (blue triangles). Magenta line indicates best fit scaling assuming 10 V_{pl}, $M = T^{1.76}$ x $10^{20.5}$. Black line shows the best fit scaling assuming 3 V_{pl}, $M = T^{1.34}$ x $10^{20.2}$.

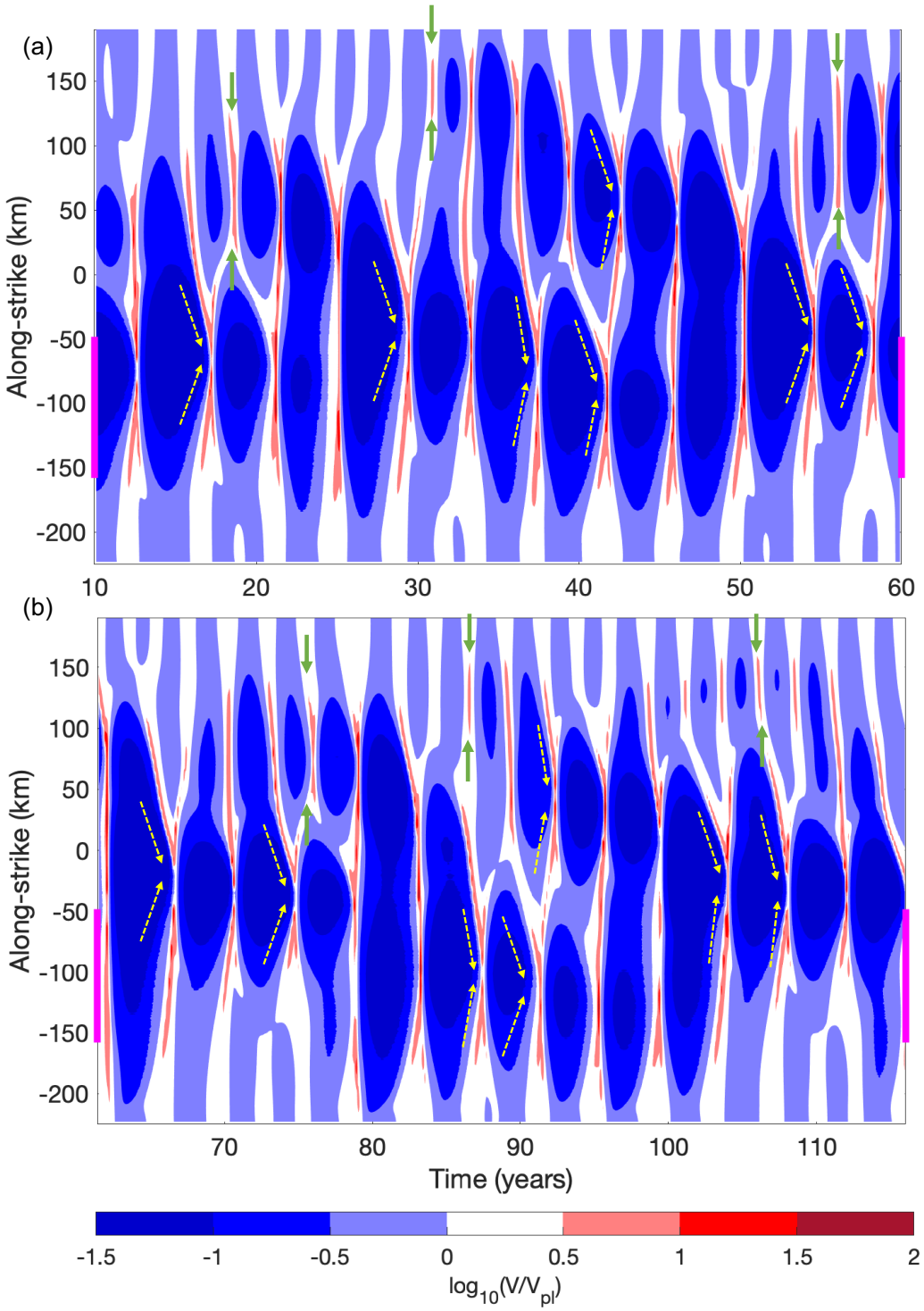

Figure S8. Spatio-temporal evolution of slip rate at 30 km depth in $\log_{10}(V/V_{pl})$ scale. Results correspond to model setup without velocity-strengthening bands on the sides of the model geometry (Text S2), the model assumes a constant $a-b$ distribution along-strike. Yellow dashed arrows indicate convergent slip fronts, most of which merge in the eastern part of the model geometry (y < 0 km). Green arrows show the SSEs with the shortest along-strike extent, which concentrate on the western part of the fault (y > 0 km)

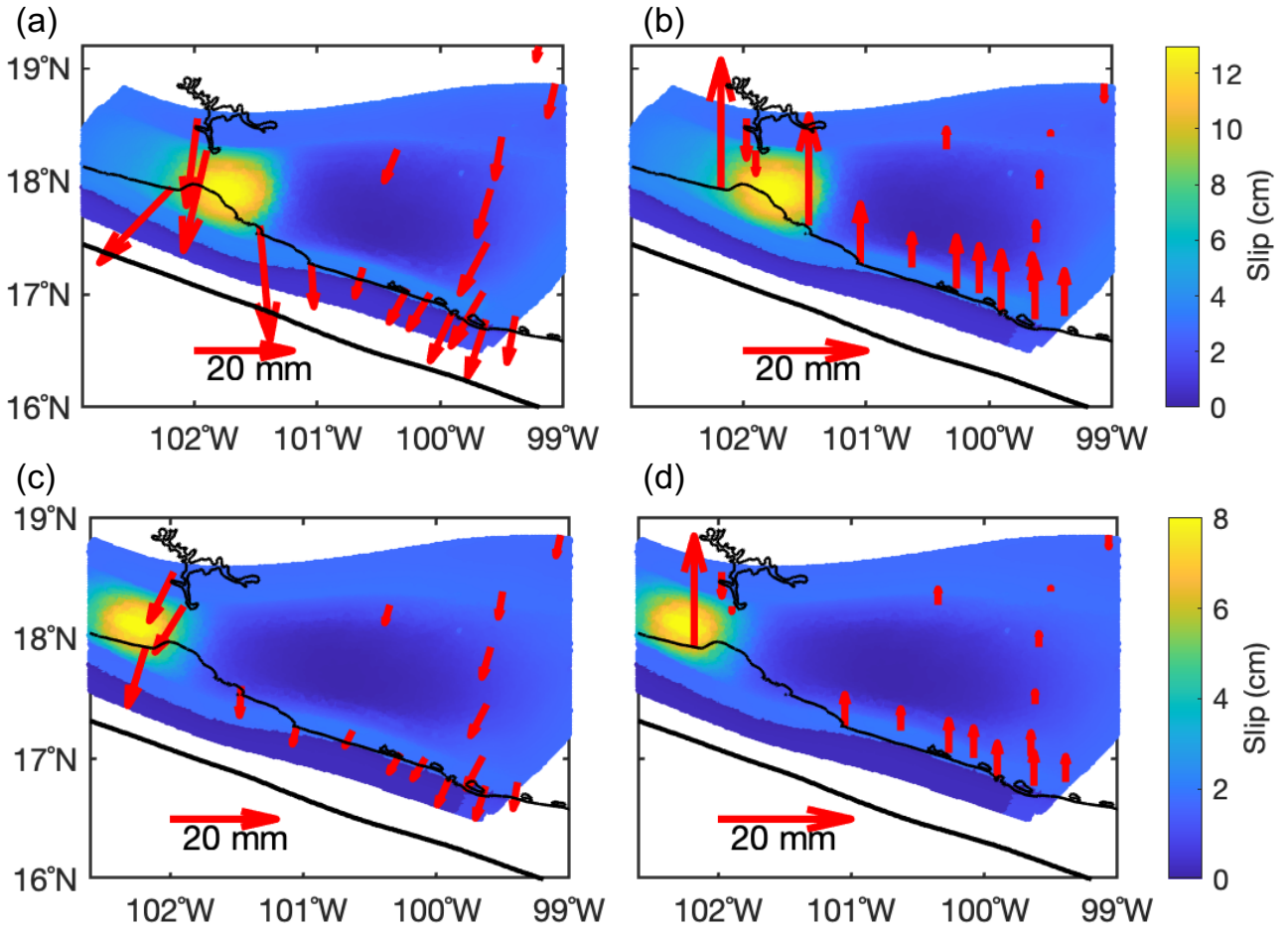

Figure S9. Synthetic GPS displacement of two representative Type III SSEs, one with significant slip (a and b) and one with small slip (c and d), from the preferred model. Synthetic displacement was calculated using the MATLAB code from Meade (2007) (see Methods in main text). Left and right column show respectively the horizontal and vertical component of displacement. Thick black line denotes the location of the trench. The cumulative slip was calculated assuming a slip velocity threshold of 3 V_{pl}. Synthetic SSE shown in (a) and (b) generated maximum surface displacements of 25.5 mm and 20 mm in the horizontal and vertical components, respectively. Also, 17 GPS station had surface displacements larger than 5 mm in the horizontal component. The second event ((c) and (d)), generated maximum displacements of 13 mm and 18 mm in the horizontal and vertical components, respectively. In addition, 11 GPS stations generated displacements larger than 5 mm.

References

DeMets, C., Gordon, R. G., & Argus, D. F. (2010). Geologically current plate motions. *Geophysical Journal International*, *181*(1), 1-80. doi: 10.1111/j.1365-246X.2009.04491.x

Dieterich, J. (1979). Modeling of rock friction 1. Experimental results and constitutive equations. *Journal of Geophysical Research*, *84*(B5), 2161–2168. doi: 10.1029/JB084iB05p02161

Dieterich, J. (2007). Applications of rate-and state-dependent friction to models of fault-slip and earthquake occurrence. *Treatise on Geophysics*, *4*, 107–129. doi: 10.1016/B978-044452748-6.00065-1

Graham, S., DeMets, C., Cabral-Cano, E., Kostoglodov, V., Rousset, B., Walpersdorf, A., … Salazar-Tlaczani, L. (2016). Slow Slip History for the MEXICO Subduction Zone: 2005 Through 2011. *Pure and Applied Geophysics*, *173*, 3445–3465. doi: 10.1007/978-3-319-51529-8_13

Li, D., & Liu, Y. (2016). Spatiotemporal evolution of slow slip events in a nonplanar fault model for northern Cascadia subduction zone. *Journal of Geophysical Research: Solid Earth*, *121*(9), 6828–6845. doi: 10.1002/2016JB012857

Meade, B. J. (2007). Algorithms for the calculation of exact displacements, strains, and stresses for triangular dislocation elements in a uniform elastic half space. *Computers and Geosciences*, *33*(8), 1064-1075. doi: 10.1016/j.cageo.2006.12.003

Radiguet, M., Cotton, F., Vergnolle, M., Campillo, M., Walpersdorf, A., Cotte, N., & Kostoglodov, V. (2012). Slow slip events and strain accumulation in the Guerrero gap, Mexico. *Journal of Geophysical Research: Solid Earth*, *117*, B04305. doi: 10.1029/2011JB008801

Radiguet, M., Perfettini, H., Cotte, N., Gualandi, A., Valette, B., Kostoglodov, V., … Campillo,

M. (2016). Triggering of the 2014 M_w 7.3 Papanoa earthquake by a slow slip event in Guerrero, Mexico. *Nature Geoscience*, *9*(11), 829–833. doi: 10.1038/ngeo2817

Rice, J. R. (1993). Spatiotemporal complexity of slip on a fault. *Journal of Geophysical Research*, *98*(B6), 9885–9907. doi: 10.1029/93JB00191

Rubin, A. M., & Ampuero, J.-P. (2005). Earthquake nucleation on (aging) rate and state faults. *Journal of Geophysical Research*, *110*, B11312. doi: 10.1029/2005JB003686

Ruina, A. L. (1983). Slip instability and state variable friction laws. *Journal of Geophysical Research*, *88*(B12), 10,359-10,370. doi: 10.1029/JB088iB12p10359

Walpersdorf, A., Cotte, N., Kostoglodov, V., Vergnolle, M., Radiguet, M., Santiago, J. A., & Campillo, M. (2011). Two successive slow slip events evidenced in 2009–2010 by a dense GPS network in Guerrero, Mexico. *Geophysical Research Letters*, *38*(15). doi: 10.1029/2011GL048124